Short-Range Inverse-Square Law Experiment in Space

Donald M. Strayer
Jet Propulsion Laboratory, Caltech, Pasadena, CA 91109
Ho Jung Paik and M. Vol Moody
Department of Physics, University of Maryland, College Park, MD 20742

The objective of ISLES (Inverse-Square Law Experiment in Space) is to perform a null test of Newton's law on the ISS with a resolution of one part in 10^5 at ranges from 100 μm to 1 mm. ISLES will be sensitive enough to detect axions with the strongest allowed coupling and to test the string-theory prediction with $R \geq 5$ μm. To accomplish these goals on the rather noisy International Space Station, the experiment is set up to provide immunity from the vibrations and other common-mode accelerations. The measures to be applied for reducing the effects of disturbances will be described in this presentation. As designed, the experiment will be cooled to less than 2 K in NASA's low temperature facility the LTMPF, allowing superconducting magnetic levitation in microgravity to obtain very soft, low-loss suspension of the test masses. The low-damping magnetic levitation, combined with a low-noise SQUID, leads to extremely low intrinsic noise in the detector. To minimize Newtonian errors, ISLES employs a near-null source of gravity, a circular disk of large diameter-to-thickness ratio. Two test masses, also disk-shaped, are suspended on the two sides of the source mass at a distance of 100 μm to 1 mm. The signal is detected by a superconducting differential accelerometer, making a highly sensitive sensor of the gravity force generated by the source mass.

1. Objectives of ISLES

The Newtonian inverse-square law ($1/r^2$ law) of gravity is a cornerstone of General Relativity (GR). Its validity has been impressively demonstrated by astronomical observations in the solar system, exceeding a level of sensitivity for violations of one part in 10^8 at $10^7 \sim 10^9$ km. In the wake of interests in searching for a "fifth force," the past two decades has seen increased activities on Earth in testing the $1/r^2$ law on the laboratory and geological scales. The experimental limit at ranges of 1 cm ~ 10 km now stands at one part in $10^3 \sim 10^4$. However, due to difficulties associated with designing sensitive short-range experiments, the range below 1 mm has been left largely unexplored (Adelberger *et al.*, 1991).

Figure 1 shows the existing limit for tests of the $1/r^2$ law at ranges below 1 mm and the expected sensitivity of our proposed experiment ISLES for the International Space Station (ISS), plotted as a function of range λ, where the total potential is written as

$$V(r) = -\frac{GM}{r}(1 + \alpha e^{-r/\lambda}). \quad (1)$$

Violations predicted by various theories are also indicated. The expected resolution of ISLES on the ISS is $|\alpha| = 1 \times 10^{-5}$ at λ = 100 μm - 1 mm and $|\alpha| = 1 \times 10^{-2}$ at λ = 10 μm. At 100 μm, this represents an improvement over the existing limits (Hoyle *et al.*, 2001) by over six orders of magnitude. ISLES reaches four orders of magnitude beyond the level aimed at by Long *et al.* (1999) in their ongoing laboratory experiment. The improvement at ranges less than 100 μm is even greater. As indicated on Fig. 1, the ISLES experiment is capable of detecting the axion with highest allowed coupling ($\theta = 3 \times 10^{-10}$), and

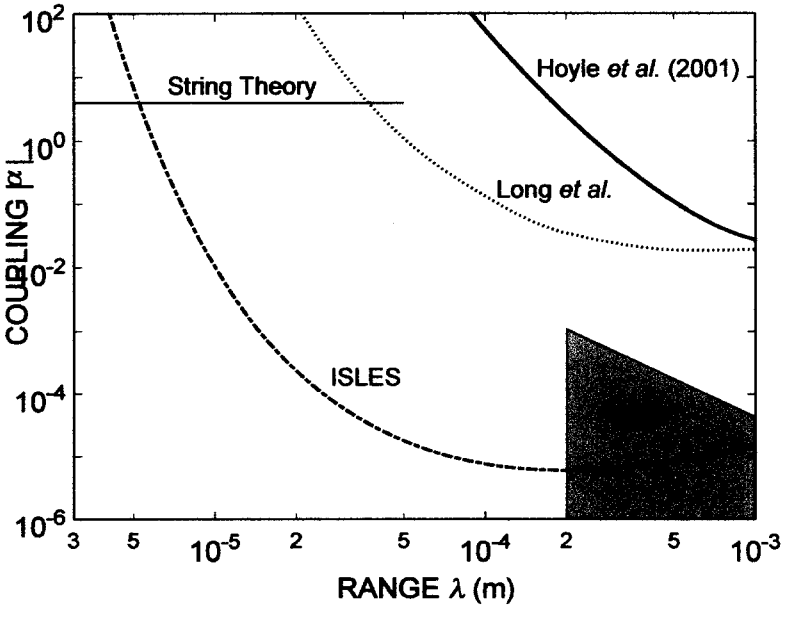

Figure 1. Sensitivity of ISLES and the existing limits

will test a string theory prediction with $R_2 \geq 5$ μm. ISLES is based on the superconducting gravity gradiometer technology fully developed at the University of Maryland (Moody *et al.*, 2002).

However, obtaining the sensitivities displayed in Fig. 1 for ISLES on the ISS is a nontrivial task. The v i-bration environment observed on the ISS, as seen in the data presently being transmitted down from orbit, is over 100 times worse than that observed in an Earth-bound laboratory. The techniques we intend to apply to reach the sensitivities depicted in Figure 1 are the main topics of this paper. Again, we shall be describing techniques that have been developed earlier for other experiments at the University of Maryland, techniques that will be adapted to the ISS for ISLES.

2. Scientific Value of Short-Range $1/r^2$ Law Test

Test of General Relativity. Existence of a short-range mass-mass interaction implies a violation of the $1/r^2$ law, a cornerstone of GR. Such a force may, or may not, have composition dependence. Therefore, the $1/r^2$ law could be violated even when the Equivalence Principle (EP) holds rigorously. So ISLES will complement STEP (Satellite Test of the Equivalence Principle) and other EP experiments that aim at testing the EP to high resolution at ranges near the Earth's radius or longer, $\lambda \geq 10^4$ km.

Test of string theories. String theories can be consistently formulated only in nine spatial dimensions. Because the space we observe is three-dimensional, the extra dimensions must be somehow hidden. If there are n compact dimensions with radii $R_1, R_2, \ldots R_n$, Gauss's law implies that the Planck mass M_{Pl} is related to a fundamental scale M_* by

$$M_{Pl}^2 \sim M_*^{2+n} R_1 R_2 \ldots R_n \,. \qquad (2)$$

In the string theory, as we reduce the distances probed to shorter than one of the radii R_i, a new dimension opens up and changes the r-dependence of the gravitational force law.

One theoretically well-motivated value for M_* is 1 TeV, which solves the gauge hierarchy problem, namely, gravity is so weak compared to the other forces. For two large dimensions of similar size, one obtains $R_1 \sim R_2 \sim 1$ mm (Arkani-Hamed *et al.*, 1999). Cosmological and astrophysical constraints give a bound $M_* > 100$ TeV (Cullen and Perelstein, 1999; Hall and Smith, 1999), while the most stringent bound, $M_* > 1700$ TeV, comes from the evolution of neutron stars (Hannestad and Raffelt, 2002). This most stringent bound corresponds to $R_1 \sim R_2 < 40$ nm. While this range is beyond the reach of ISLES, there are co smological assumptions going into these bounds, and a null result from ISLES would supply independent confirmation of the model being tested.

Search for the axion. The Standard Model of particle physics successfully accounts for all existing particle data; however, it has one serious blemish: the strong *CP* problem. Strong interactions are such that parity (*P*), time reversal (*T*), and charge conjugation (*C*) symmetries are automatically conserved in perturbation theory. However, non-perturbative effects induce violations of *P* and *CP* (parameterized by a dimensionless angle θ), but no such violations have been observed in strong interactions. Peccei and Quinn (1977) developed an attractive resolution of this problem. One ramification of their theory is the existence of a new light-mass boson, the *axion* (Weinberg, 1978; Wilczek, 1978). The axion mediates a short-range mass-mass interaction. The experimental upper bound $\theta \leq 3\ 10^{-10}$ corresponds to a violation of the $1/r^2$ law at the level of $|\alpha| \sim 10^{-4}$ at $\lambda = 1$ mm, a force strength that is within reach for ISLES as depicted in Fig. 1.

The axion could also solve the major open question in astrophysics: the composition of dark matter. Galactic rotation curves and inflation theory require that there should be more mass in the universe than is observed. Although neutrino mass, MACHOs (MAssive Compact Halo Objects), and many hypothetical particles have been offered as explanations, the solution remains elusive. The axion is one of the strongest candidates for the cold dark matter (Turner, 1990).

3. Principle of the Experiment

Newtonian null source. To maximize the masses that can be brought to distances of 100 μm from each other, flat disk geometry is used for both the source and test masses, as is done by Long *et al.* (1999). An infinite plane slab is a Newtonian null source in that the gravity force it exerts on a nearby mass does not depend on the distance between the mass and the slab. We approximate such a null source by using a circular disk of sufficiently large diameter. Figure 2 shows the configuration of the source and test masses with associated coils and capacitor plates.

Levitated test masses. Two disk-shaped superconducting test masses are suspended on the two sides of the source mass using magnetic forces and are coupled magnetically to form a differential accelerometer. The motions induced in the test masses are detected by sensing coils (L_{S1} and L_{S1}) in Figure 2.

On Earth it is difficult to suspend two flat disks on opposite sides of the source mass at such proximity without significantly modifying the geometry and stiffening the differential mode, thus degrading the resolution of the experiment. In microgravity on the ISS, each test mass can be suspended by applying only minute forces from a pancake coil (L_{S1} or L_{S2}) and from a small ring coil (L_{R1} or L_{R2}) coupled to a narrow slanted rim of the test mass.

Second harmonic detection. As the source mass is driven at frequency f_S along the symmetry axis, the first-order Newtonian fields arising from the finite diameter of the source mass are canceled upon differential measurement, leaving only a second-order error at $2f_S$. By symmetry, the Yukawa signal also appears at $2f_S$. The second harmonic detection, combined with the common-mode rejection ratio (CMRR) of the detector, reduces source-detector vibration coupling by over 300 dB.

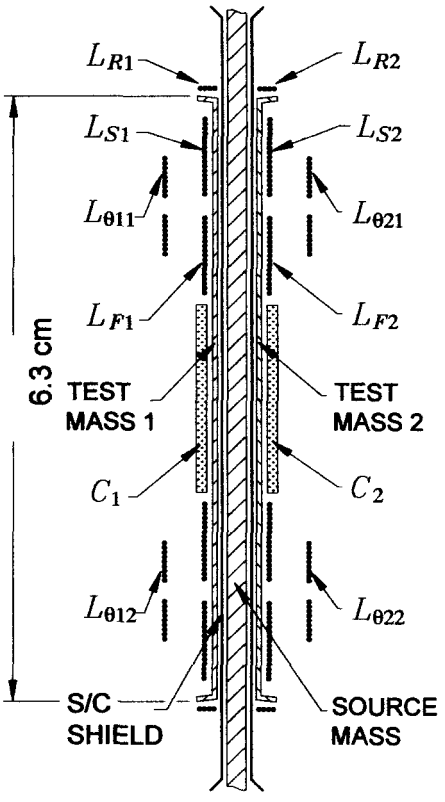

Figure 2. Configuration of the source and test masses.

Expected signal. The design allows a source displacement of ±50 μm. The differential acceleration signals expected from the Newtonian force (with correction to 10%) and the Yukawa force with $|\alpha| = 10^{-5}$ and $\lambda = 100$ μm are plotted in Figure 3 as a fun c- tion of the source mass position. The rms amplitude of the Yukawa signal corresponding to a ±50-μm displacement is 1.2×10^{-11} α m/s^2. The rms amplitude of the Newtonian error term arising from the finite diameter of the source mass is 1.0×10^{-16} m/s^2 before compensation. While these force amplitudes at $2f_S$ are similar, the Newtonian error will be computed and removed to less than 10% as depicted in Fig. 3, which is straightforward.

Need for low gravity. Sensitive experiments searching for weak forces invariably require soft suspension for the measurement degree of freedom, for which superconducting magnetic levitation offers great promise. Levitation in Earth's gravity, on the other hand, requires a large magnetic field that tends to couple to the measurement axis through metrology errors, and thus stiffens the mode. The large value of magnetic field also makes the suspension more dissipative. Fields close to the critical field H_c of the superconductor must be used to levitate the masses on Earth. As well, surface impurities will reduce H_c locally. The magnetic field will also be stronger near sharp edges. These effects cause the magnetic fields to be trapped, contributing to damping of the motions through flux creep.

The situation improves dramatically in orbit. The gravity level is reduced by five to six orders of magnitude, so the test masses can be supported with weaker magnetic springs, permitting the realization of both the lowest resonance frequency and lowest dissipation. Our calculations show that, even on such a relatively noisy platform as the ISS, the space experiment will have at least 100 times better resolution over the ground experiment.

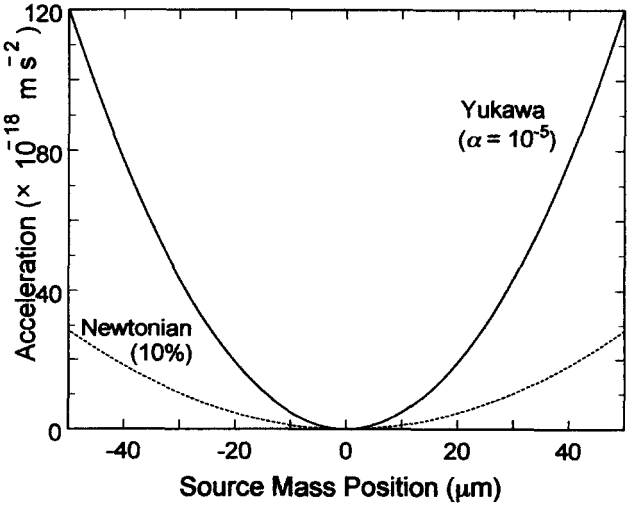

Figure 3. Newtonian and Yukawa signals versus source position.

4. Experimental Hardware

Overview of the apparatus. Figure 4 shows a cross-sectional view of the apparatus. The entire housing is fabricated from niobium (Nb). The source mass is made out of tantalum (Ta), which closely matches Nb in thermal contraction. This source disk is suspended by cantilever springs at the edge and driven magnetically. A thin Nb shield provides electrostatic and magnetic shielding between the source and each test mass. The test masses are suspended and aligned by magnetic fields from various coils. Two auxiliary three-axis superconducting accelerometers are mounted on opposite sides of the housing to provide linear and angular acceleration signals.

The entire assembly weighs 6.0 kg and fits within the 20-cm diameter envelope of the LTMPF instrument well (see Fig. 5). The masses need not be caged during launch and ISS maneuvers since their sway space will be limited to ±50 μm by mechanical stops. -

The ISLES cryogenic and electrical requirements will be met with the standard LTMPF provision with minor modifications. The entire apparatus is fastened to the second-stage thermal platform of the cryo-insert of LTMPF (Fig. 5). That platform and the instrument will be temperature stabilized to 5 μK. The orientation of the detector is chosen so that its sensitive axis is aligned with the pitch (y) axis of the ISS when LTMPF is mounted on JEM-EF. This orientation reduces the centrifugal acceleration noise almost a hundred-fold.

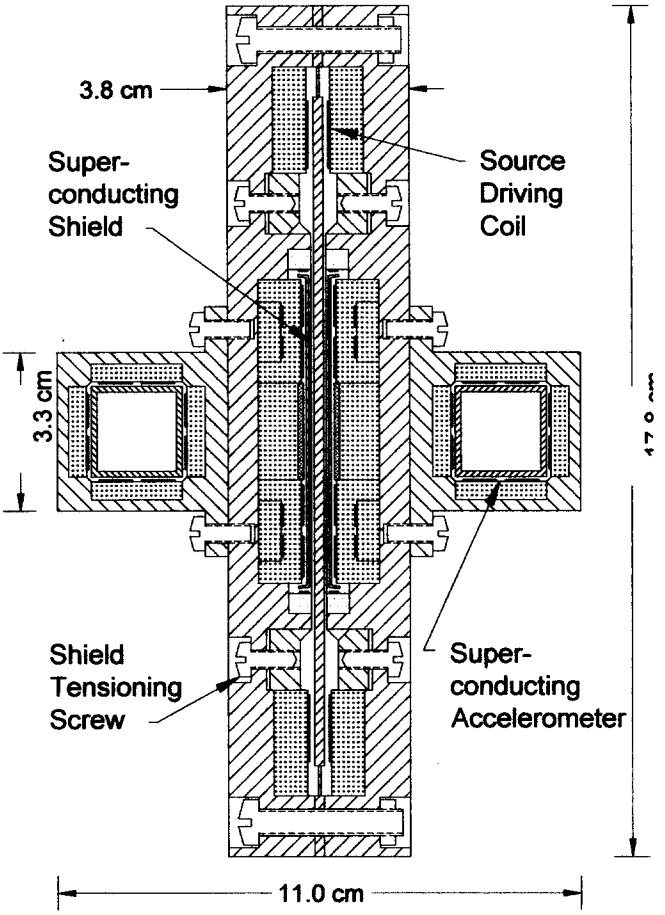

Figure 4. Cross section of the ISLES apparatus.

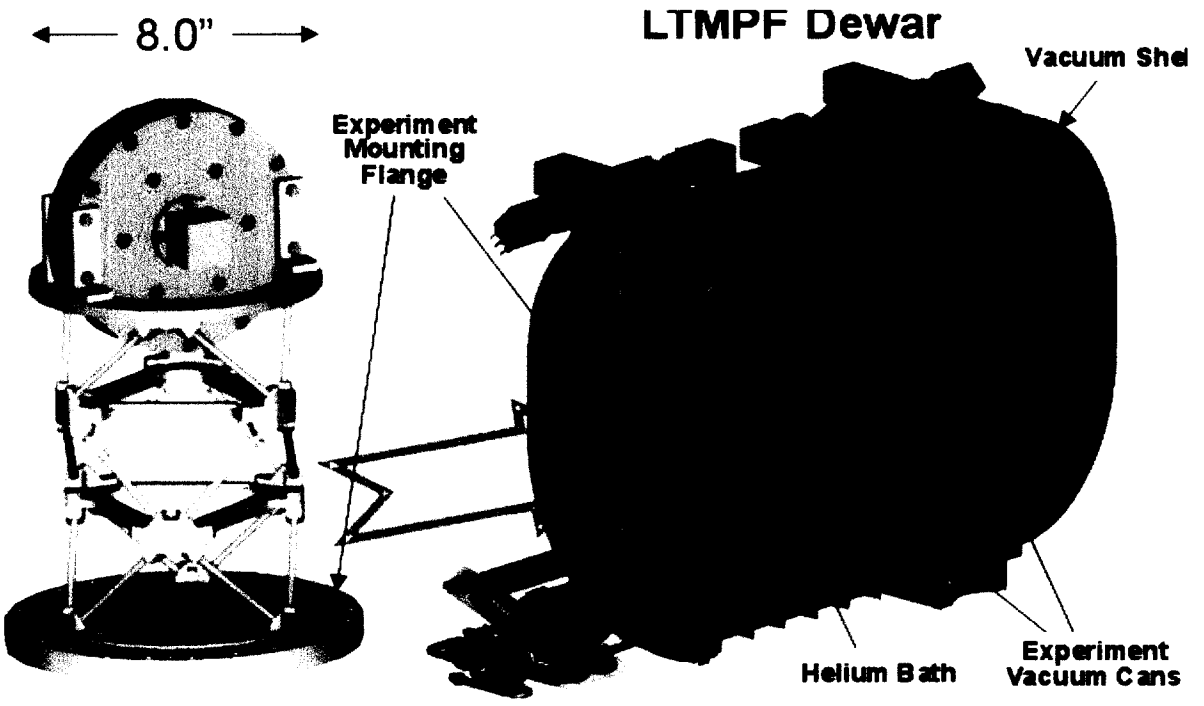

Figure 5. The ISP mounted on the Cryo Insert.

Source and test masses. The source mass is a disk 2.0 mm thick by 140 mm in diameter, with mass M = 510 g. The source mass, cantilever springs, and rim are machined out of a single plate of Ta. Ta is chosen for its high density (16.6 g cm^{-3}), which increases the signal, and its relatively high H_c. Each test mass is a Nb disk 0.25 mm thick by 63 mm in diameter, with a rim 0.25 mm thick by 2.0 mm wide, which has 5° slant from the axis. The mass of each test mass is m = 7.5 g. For the 100-μm gap, the test masses are separated by a baseline ℓ = 2.45 mm. The position of each test mass is measured by a capacitor plate located near its center (see Figure 2). The equilibrium spacing between the source and each test mass is 100 μm. They are shielded from each other by means of a 12.5-μm thick Nb shield, located at 25 μm from the su rface of the test mass. The source mass is driven magnetically by coupling a small ac current to a superconducting circuit carrying a large persistent current.

Superconducting circuitry and setup procedure. Schematics of the superconducting circuits for the detector are shown in Figure 6. These circuits are similar to the standard differencing circuit used in the SGG (Moody *et al.*, 2002). The test masses are suspended radially by storing persistent currents I_{R1} and I_{R2} in ring coils L_{R1} and L_{R2} and the pancake coils, as shown in Figure 6(a). Due to the slanted rim of the test masses, currents I_{R1} and I_{R2} will exert an axially outward force on the test masses. This force is balanced by the axially inward forces provided by the currents in the sensing, alignment, and feedback circuits, shown in Figures 6(b), (c), and (d). The suspension is stable for all degrees of freedom, except for roll about the sensitive axes.

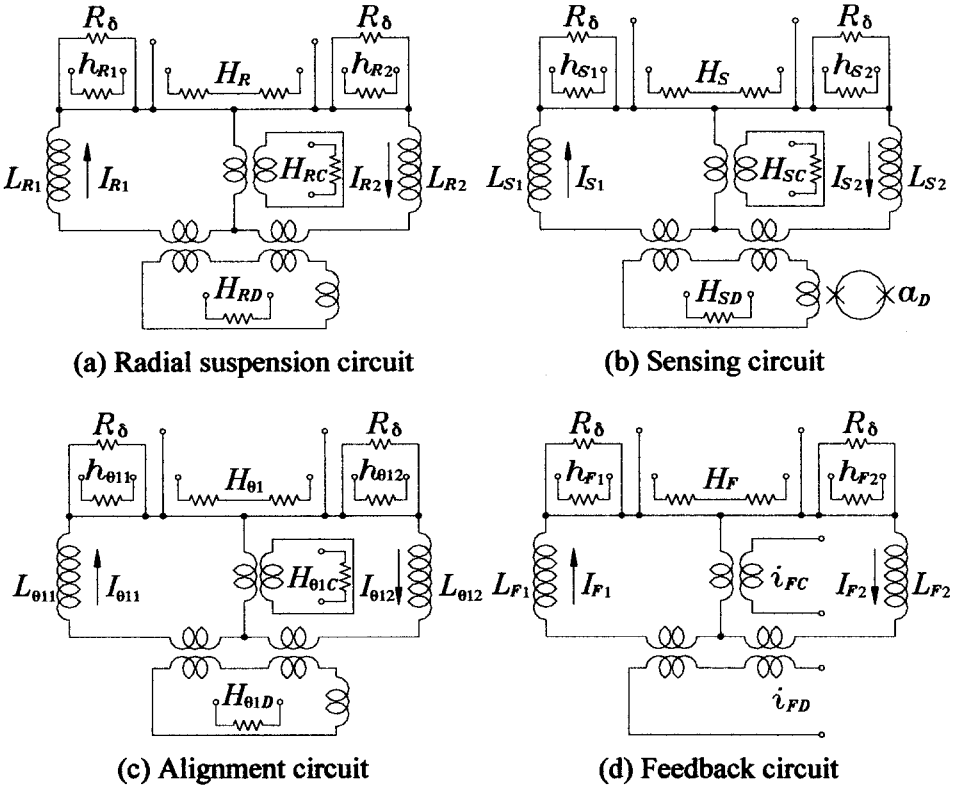

Figure 6. Superconducting circuits for the detector.

The scale factors of the component accelerometers are matched by adjusting currents I_{S1} and I_{S1} in pancake coils L_{S1} and L_{S1}, as shown in Figure 6(b). The SQUID measures the differential acceleration a_D, or gravity gradient, along the y-axis. To align an individual test mass parallel to its shield and to also align its axis parallel to the axis of the other mass, two alignment circuits are provided for each test mass, one per degree of freedom. Figure 6(c) shows the alignment circuit of test mass 1 about the x-axis. This alignment is accomplished by tuning currents $I_{\theta 11}$ and $I_{\theta 12}$ in remotely coupled pancake coils $L_{\theta 11}$ and $L_{\theta 12}$ (see also Figure 2). Note that the unique property of long-term stability of persistent currents in superconductors preserves the CMRR tuning over long periods.

The balance procedure matches the linear components of the scale factors but does not completely match the nonlinearity. This mismatched nonlinearity is troublesome since it down-converts the wide-band acceleration noise to the signal frequency. A standard approach to suppressing the nonlinearity is applying a negative feedback to the test masses, which *actively* stiffens the mode. The feedback circuit is given in Figure 6(d). The common-mode (CM) and differential-mode (DM) outputs i_{FC} and i_{FD} are fed back to the test masses. The CM output is derived from the auxiliary accelerometers. Currents I_{F1} and I_{F2} are adjusted to null the effect of the CM feedback on the DM output.

Coarse and fine heat-switches. Due to the high vibration levels of the ISS (> 10^{-6} m s^{-2} Hz$^{-1/2}$), a special provision must be made to be able to control the magnetic fluxes trapped in various superconducting loops with adequate precision. Coarse heat-switches, denoted by H_{ij}'s, warm up a short length of the Nb wire to a

resistance $R \sim 1$ mΩ, resulting in an L/R time of about 10 ms. These coarse switches are used to store currents initially to obtain, for example, the desired spring constants for the suspended masses. Fine heat-switches, denoted by h_{ij}'s, couple a low-resistance path with $R_\delta \sim 0.1$ μΩ to the circuit, resulting in a time co nstant of about 100 s. With 1-ms time resolution of the heat-switch, fluxes can then be adjusted to one part in 10^5. This added precision of the trapped currents gives the ability to match the scale factors to 10^{-5} and to align the sensitive axes to 10^{-5} radian, resulting in an initial CMRR of 10^5 in all three linear degrees of freedom.

Heat-switch H_{SD} in Figure 6(b) is turned on to protect the SQUID from a current surge whenever a current is adjusted in the sensing circuit. The output heat-switches H_{iC}'s and H_{iD}'s are turned on to passively damp the corresponding modes in the event large motions of the test masses are excited. While we expect this tuning to maintain its high degree of noise rejection throughout the 5-month period of the experiment on ISS, we use the vibrationally noisy periods of Shuttle dockings and orbit reboosts, when gravity data are unusable or degraded, to test the CMRR and to readjust current values, as found necessary.

Auxiliary superconducting accelerometers. Figure 4 shows two three-axis auxiliary superconducting accelerometers mounted symmetrically on the two sides of the housing. Each test mass is a hollow 20-gram Nb cube, suspended and sensed by Nb pancake coils adjacent to its six faces. The suspension of the cube is stable in all degrees of freedom. The accelerometers are coupled to SQUIDs, two SQUIDs per degree of freedom, to measure three linear (a_i) and two angular (α_i) acceleration components, as well as a gravity gradient component (Γ_{ij}).

Figure 7 shows the superconducting circuit for the y-axis of the auxiliary accelerometers. The four pancake coils separated along the y-axis are combined to sum and difference the signals. The CM and DM signals correspond to a_y and Γ_{yy}, respectively. The gravity gradient signal is used to monitor and remove gravitational disturbances from the detector. The pancake coils separated along the x- and z-axes are combined in similar circuits to measure a_x and α_z, and a_z and α_x, respectively. The only component that is not measured is α_y, which is not needed for error compensation.

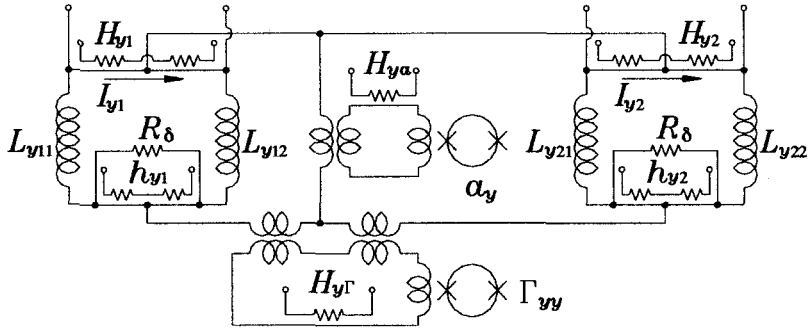

Figure 7. Superconducting circuit for the y-axis of the coupled three-axis auxiliary accelerometers.

The intrinsic noise of the accelerometers at $f = 0.02$ Hz, assuming the noise spectrum of commercial Quantum Design SQUIDs, are $S_a^{1/2}(f) \sim 1 \times 10^{-11}$ m s^{-2} Hz$^{-1/2}$, and $S_\alpha^{1/2}(f) \sim 3 \times 10^{-11}$ rad s^{-2} Hz$^{-1/2}$, and $S_\Gamma^{1/2}(f) \sim 3 \times 10^{-11}$ s^{-2} Hz$^{-1/2}$.

5. Dynamic Noise Rejection

Error compensation. Linear and angular accelerations are rejected to 10^{-5} and to 10^{-4} m, respectively, by adjusting persistent currents in the sensing and alignment circuits as described above. To improve the acceleration rejection further, we apply an error compensation technique that has been demonstrated with the SGG (Moody *et al.*, 2002). The linear and angular accelerations of the platform, measured by the auxiliary accelerometers, are multiplied by the predetermined error coefficients and subtracted from the detector output to achieve a further reduction of noise by the factor 10^3. By applying the compensation factor 10^3 demonstrated in the laboratory, we should be able to achieve a net CMRR of 10^8 for linear acceleration and a net error coefficient of 10^{-7} m for angular acceleration.

To determine the dynamic error coefficients, accelerations in all degrees of freedom must be provided. If active vibration isolation is implemented as described in the next section, a six-axis shaker will be built into the isolation system that can also be used to apply a sinusoidal acceleration signal in each degree of freedom. If we opt not to employ the vibration isolation system, we will use the ISS vibration noise itself to shake the detector. The accelerations will be random and cross-correlated between degrees of freedom. However, we

can apply a well-established procedure in electrical engineering for determining the transfer functions for a multiple-input system using noise alone (Bendat and Piersol, 1971).

Due to the short but finite baseline (ℓ = 2.45 mm), the $1/r^2$ law detector is a gravity gradiometer that is sensitive to attitude modulation of Earth's gravity gradient, gravity noise from ISS, and centrifugal accelerations. Fortunately, the auxiliary gradiometer measures exactly the same gradient noise, except for gravity disturbances from nearby objects (< 1 m). This gravity gradient noise can thus be removed from the detector output by applying the above correlation method.

Vibration isolation (option). With the residual acceleration errors compensated, the most important dynamic error source is the nonlinearity of the scale factors. Vibration isolation of the detector is an alternative way of suppressing the nonlinearity noise.

An active vibration isolation system, combined with a single-stage passive isolation, was studied for LTMPF by Ball Aerospace & Technologies Corp. (BATC). As LTMPF is designed presently, the sway space is limited to ±3 mm. This sway amplitude limit constrains our ability to extend the isolation to below 0.1 Hz. Eight D-strut isolators were used to attach the facility frame to the Payload Interface Unit (PIU). These isolators provide a 40-dB/decade attenuation from 1 to 200 Hz. Each isolator is also equipped with a voice-coil actuator to provide active isolation. The outputs of the superconducting accelerometers are fed back to these actuators.

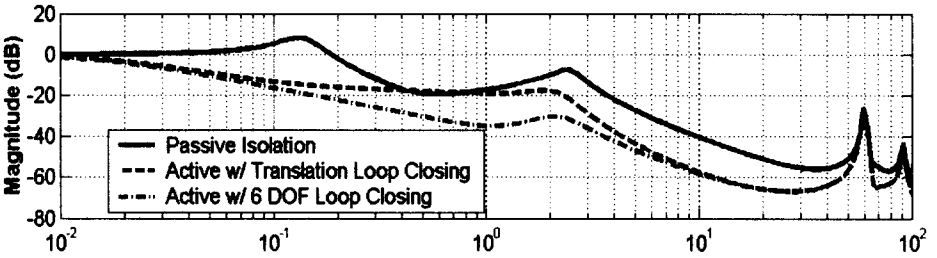

Figure 8. Frequency response of the vibration isolation system for *y*-axis.

The result is shown in Figure 8. The first curve (blue) is the passive isolation provided by the eight D-strut isolators. The first active system shown as the green curve employs only control over the translation degrees of freedom. The second active system (red curve) employs closed-loop control over all six degrees of freedom. The isolation system provides only a 10-dB isolation at 0.05 Hz. Its main advantage comes from the reduction of high-frequency acceleration noise, reducing the nonlinearity noise.

6. Error Budget

Metrology errors. Table 1 lists the metrology errors estimated using a numerical model. The effects from the finite diameter of the source and the dynamic mass of the suspension springs are corrected to 10% and 20%, respectively. Linear taper and linear density variation of the source produce second-order errors, which become negligible. The test masses tend to rotate slowly about the sensitive axis, further averaging out the asymmetry about the axis. Hence only the radial taper and the radial density variation are important. Due to the null nature of the source, test mass metrology is not important, except for the extended rim. The rim dimension is corrected to 2.5 μm. The requirements on radial positioning of the test masses are greatly relaxed by the cylindrical symmetry. The total metrology error is 1.5×10^{-17} m/s^2.

Source	Allowance	Error ($\times 10^{-18}$ m s^{-2})
Baseline	25 μm	1.0
Source mass		
Finite diameter	10%	12
Suspension spring	20%	2.4
Radial taper	2.5 μm	7.8
Radial density variation	10^{-4}	0.2
Test masses		
Rim dimension	2.5 μm	1.7
Total error		15

Table 1. Metrology errors

The dimensional tolerances are achievable using hand lapping of the parts. Fabrication of the test masses with a slanted rim will require a special procedure. One possibility is machining the entire structure in a single piece by combining regular machining with electric discharge machining (EDM). Another possibility is machining the disk and the rim as separate pieces and then diffusion-bonding them in a vacuum oven.

Intrinsic instrument noise. The intrinsic power spectral density of a superconducting differential accelerometer can be written (Chan and Paik, 1987; Moody *et al.*, 2002) as

$$S_a(f) = \frac{8}{m}\left[\frac{k_B T \omega_D}{Q_D} + \frac{\omega_D^2}{2\eta\beta} E_A(f)\right], \tag{3}$$

where m is the mass of each test mass, $\omega_D = 2\pi f_D$ and Q_D are the differential mode resonance frequency and quality factor, β is the electromechanical energy coupling coefficient, η is the electrical energy coupling coefficient of the SQUID, and $E_A(f)$ is the input energy resolution of the SQUID.

Equation (3) shows that the differential-mode frequency f_D is a critical parameter for the intrinsic noise. The microgravity environment on ISS, in principle, allows a suspension 10^6 times softer than on the ground, which corresponds to $f_D < 0.01$ Hz. On the other hand, the differential accelerometer's response to platform vibrations must be minimized to reduce errors caused by electric charge on the test mass, by patch-effect fields, by self-gravity of the ISS, and most importantly by the nonlinearity of the scale factors. Ideally, one would like to increase the common-mode frequency f_C as much as possible, while keeping f_D low. Unfortunately, the nonlinearity of the coils couples a fraction of the CM stiffness to DM, providing a practical limit: $f_C/f_D \leq 4$. This limitation forces us to make a compromise. The test masses must remain free before a feedback loop is closed either to the test masses or to the isolator, since otherwise there will be no signal to feed back. Moreover, we need to keep the test mass excursion to ≤ 10 μm. These considerations require $f_C \geq 0.2$ Hz and $f_D \geq 0.05$ Hz. The result represents a stiffness reduction by 10^4 from the ground experiment.

Analysis of ISLES circuits for the masses chosen shows that $I_{11} = I_{21} \approx 4.7$ mA and $I_{13} = I_{23} \approx 47$ mA gives $f_D = 0.05$ Hz and $f_C = 0.2$ Hz. For feedback operation of the detector, this choice of mode frequencies, with signal frequency $f = 0.02$ Hz, minimizes the total dynamic noise. The radial translational mode frequency is found to be ~ 0.06 Hz. The test masses are free to roll about their axes. Rolling will tend to average out azimuthal asymmetries of the source and the test masses. If active vibration isolation is provided, the optimum frequencies shift slightly to $f = 0.05$ Hz, $f_D = 0.1$ Hz and $f_C = 0.4$ Hz. We compute the intrinsic noise for these two sets of frequencies.

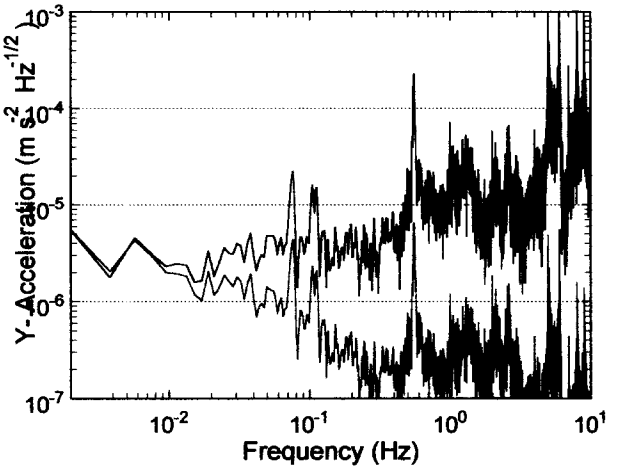

Figure 9. Linear acceleration along *y*-axis: actual (upper) and with active isolation (lower).

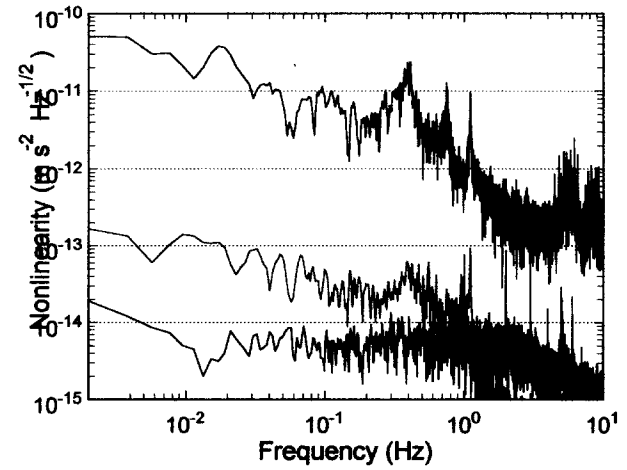

Figure 10. Nonlinearity error for *y*-axis: actual (upper), with active isolation (middle), and with

The design values for the other parameters of Eq. (3) are: $T = 2$ K, $m = 7.5$ g, $Q_D = 10^6$, $\beta = \eta = 0.5$, and $E_A(f) = 10^{-30}\,(1 + 0.1\ \text{Hz}/f)$ J Hz^{-1}. The SQUID energy resolution corresponds to the flux noise, 5 $\mu\Phi_0$ Hz$^{-1/2}$, originally specified in LTMPF Science Requirement Document, and coincides with the performance typically obtained from commercially available dc SQUIDs. We assume that this SQUID noise level can be achieved for ISLES. With the above parameter values, we find $S_a^{1/2}(f) = 7.0 \times 10^{-14}$ m s^{-2} Hz$^{-1/2}$ for $f = 0.02$ Hz and $f_D = 0.05$ Hz (for feedback), and $S_a^{1/2}(f) = 10.8 \times 10^{-14}$ m s^{-2} Hz$^{-1/2}$ for $f = 0.05$ Hz and $f_D = 0.1$ Hz (for vibration isolation).

Acceleration Noise. The upper curve of Figure 9 shows the *y*-axis linear acceleration spectrum measured by a SAMS II accelerometer in the US Lab of ISS on a typical day. The lower curve is the acceleration spectrum with active isolation, the curve being generated by filtering the acceleration spectrum with the response function given in Figure 8. The noise is quietest at ~ 0.01 Hz, with a value of 3×10^{-6} m s^{-2} Hz$^{-1/2}$. This noise will be reduced to 3×10^{-14} m s^{-2} Hz$^{-1/2}$ by the net CMRR of 10^8. The angular acceleration noise is reduced to 2×10^{-14} m s^{-2} Hz$^{-1/2}$ by the error coeff i-cient of 10^{-7} m. The centrifugal acceleration noise is negligible.

Using the nonlinearity coefficient measured in the SGG (Moody *et al.*, 2002), we estimate the nonlinearity-induced noise as plotted in Figure 10. The upper curve is the noise without active isolation or feedback, which is 10^3 times higher than the intrinsic noise of the

instrument at 0.01 Hz. The middle curve shows the result of applying the active isolation. At 0.01 Hz, the nonlinearity noise is at 1×10^{-13} m s^{-2} Hz$^{-1/2}$. The lower curve shows the nonlinearity noise expected in the detector under a feedback control that stiffens the common mode frequency to 10 Hz.

Assuming that the above acceleration noise represents the actual noise that will be experienced by the ISLES detector, we find a total acceleration noise to be 6.3×10^{-14} m s^{-2} Hz$^{-1/2}$ at $f = 0.02$ Hz for the feedback option, and 5.9×10^{-14} m s^{-2} Hz$^{-1/2}$ at $f = 0.05$ Hz for the vibration isolation option.

Gravity noise. Helium tide is absent due to the Earth-fixed orientation of the ISS. Helium sloshing is of minor concern since it is expected to occur at a sufficiently low frequency, ~2.5 mHz. The gravity gradiometer along the x-axis will be used to monitor gravitational disturbances of the experiment. The gravity noise from modulation of the Earth's gravity gradient and ISS self-gravity, including the activities of astronauts, will be taken out, along with the centrifugal acceleration, by the error measurement and compensation scheme.

Magnetic crosstalk. Trapped flux is not of concern if the flux is strongly pinned. Cooling and performing the experiment in a low magnetic field will minimize flux creep. For this purpose, LTMPF is equipped with a Cryoperm shield. Material processing and the insertion of flux dams can reduce flux motion that might be induced by the incidence of charged particles in orbit.

With the high magnetic field required to drive the source mass, magnetic crosstalk between the source and the detector is a very important potential source of error. To solve this problem, the entire housing is machined out of Nb and a Nb shield is provided between the source and each test mass. High-purity Nb will be used. The Nb will be heat-treated to bring the material very close to a type-I superconductor, thus minimizing flux penetration. The superconducting shield is expected to provide over 200 dB isolation (Rigby *et al.*, 1990). This isolation, combined with 60 dB rejection expected from the second harmonic detection, should provide the required isolation between the source drive signal and the test masses in excess of 260 dB.

Electric charge effects. Levitated test masses in orbit will accumulate electric charge from cosmic rays and from high-energy protons, as the spacecraft traverses through the South Atlantic Anomaly. Scaling from the charge computed for STEP test masses (Blaser *et al.*, 1996), we find that the total charge accumulated in each ISLES test mass over the entire duration of the experiment will be $Q \approx 1.5 \times 10^{-13}$ C. In deriving this number, we used a charge trapping efficiency 10% that of STEP to account for the difference in shape: the ISLES test masses are extremely thin (250 μm) and do not trap charge as efficiently as the much thicker STEP test masses.

The charge trapped in the test mass will induce image charges on the neighboring coils and superconducting ground planes. Most of the trapped charge will appear on the surfaces of the test masses facing the shields since the gap is smallest there (~ 20 μm). This will generate a differential force $Q^2/\varepsilon_0 A$, where ε_0 is the permittivity of vacuum and A is the area of the test mass. The force results in the maximum differential displacement at the end of the mission:

$$x_{D,\max} = \frac{Q^2}{\varepsilon_0 A} \frac{1}{m\omega_D^2} \approx 7 \times 10^{-9} \text{m}. \tag{4}$$

A differential displacement affects the CMRR through mismatches in the coil areas, gaps, and currents. With the initial coil gap of 10^{-4} m and a mismatch of 10%, we find that the CMRR is affected by 7 ppm at most. This should allow the passive CMRR to remain at the required level of 10^5 throughout the mission. So ISLES does not require a discharging system. To make sure that the trapped charge remains below the threshold, the charge will be measured after each 30-day data run and the test masses will be discharged, if necessary, by simply pushing it against the shields. This may necessitate a recalibration of the detector.

The energetic charged particles will also impart momentum and cause heating of the test masses. These effects were found to be less important than the electrostatic force for STEP. In addition, patch-effect potential will be modulated as charge builds up in the test masses, causing a time-varying acceleration. These ac disturbances occur mostly outside the signal band and therefore are averaged out. The Casimir force is not of concern for the present experiment where the gap between the masses is >> 1 μm (Lamoreaux, 1997).

Temperature noise. The modulation of the penetration depth of a superconductor with temperature and residual thermal expansion coefficients for different materials give rise to temperature sensitivity in a superconducting accelerometer. These occur through temperature gradients as well as mismatches in the acceler-

ometers (Chan and Paik, 1987). From our experience with the SGG, however, this noise is expected to be negligible with the platform temperature stabilized to 5 μK.

Total errors. Table 2 combines all the errors for the two scenarios: one with feedback and the other with vibration isolation. To reduce the random noise to the levels listed, a 90-day integration was assumed. The vibration isolation approach does not reduce the total noise, but is worth considering because it greatly simplifies the detector design and operation. It allows the use of a slightly stiffer suspension, which will reduce the disturbances from the trapped charge. Therefore, we plan to have a trade study at the beginning of the flight definition phase, comparing the risks and benefits, and the costs of implementing these approaches.

Error Source	Error ($\times 10^{-18}$ m s^{-2})	
	w/ feedback	w/ isolation
Metrology	15	15
Random	(90 days)	(90 days)
Intrinsic	25	39
ISS vibration	23	21
Gravity noise	< 1	< 1
Vibration coupling	< 1	< 1
Magnetic coupling	< 10	< 10
Electric charge	< 10	< 10
Other (30% margin)	33	41
Total	52	64

Table 2. Error budget.

7. Expected Resolution

By equating the noise with the expected Yukawa signal, we compute the minimum detectable $|\alpha|$. Figure 1 shows the 1-σ error plotted as a function of λ for the feedback approach. The case with active isolation is very similar. The best resolution of ISLES is $|\alpha| = 1 \times 10^{-5}$ at $\lambda = 100$ μm ~ 1 mm. ISLES will test the $1/r^2$ law with a resolution of 10^{-2} at $\lambda = 10$ μm. Figure 1 shows that the string theory predicted violation with $R_2 \geq 5$ μm will be detected and axions with strength 10 ~100 times below the maximum will be detected.

ISLES will use the SGG technology fully developed at the University of Maryland. The SGG has been used to perform a null test of Newton's law at a sensitivity ten times beyond that of the other methods at 1-meter distance (Moody and Paik, 1993). The instrument proposed for ISLES is very similar to the existing SGG and will apply noise-compensating techniques already demonstrated on the SGG. The experimental procedure and error analysis are also similar to those in the meter-scale $1/r^2$ law test, also previously carried out with the SGG.

For the modest cost of the ISS experiment, the scientific gain from ISLES is tremendous. ISLES constitutes a new test of General Relativity in the hitherto largely untested range and will perform the first ever test of a prediction of string theory. The experiment will push the frontiers of searching for new weak forces by several orders of magnitude, with a potential to discover new particles.

It should be noted that the instrument will launch while completely inactive, with no currents stored and no electronics turned on. Once on orbit, the SQUIDs and the temperature control circuits will be activated, and the 'levitation' currents will be set. Then the tuning of the CMRR will proceed, and the error coefficients will be measured. With these data stored, the data for testing the $1/r^2$ law can be gathered. This passive launch implies that no exchange gas need be placed in the vacuum space during launch, so the lowest possible residual gas levels will be obtained in the space around the instrument. Thus, high Q-values can be expected for the test mass motions. Also, being able to adjust all experimental parameters while the instrument is on orbit means that the experimenter is able to monitor and correct any error-inducing disturbances that might occur during the experiment's tenure.

References

Adelberger, E. G. *et al.* (1991), *Ann. Rev. Nucl. Part. Sci.* **41**, 269.

Arkani-Hamed, N., Dimopoulos, S., and Dvali, G. (1999), *Phys. Rev. D* **59**, 086004.

Blaser, J.-P. *et al.* (1996), *STEP (Satellite Test of the Equivalence Principle)*, Report on the Phase A Study, SCI(96)5.

Bendat, J. S. and Piersol, A. G. (1971), *Random Data: Analysis and Measurement Procedures* (Wiley, New York), Chapter 5.

Chan, H. A. and Paik, H. J. (1987), *Phys. Rev. D* **35**, 3551.

Cullen, S. and Perelstein, M. (1999), preprint hep-ph/9903422.

Hall, L. J. and Smith, D. (1999), *Phys. Rev. D* **60**, 085008.

Hannestad, S. and Raffelt, G. G. (2002), *Phys. Rev. Lett.* **88**, 071301.

Hoyle, C. D. *et al.* (2001), *Phys. Rev. Lett.* **86**, 1418.

Lamoreaux, S. K. (1997), *Phys. Rev. Lett.* **78**, 5.

Long, J. C. *et al.* (1999), *Nucl. Phys. B* **539**, 23.
Moody, M. V. and Paik, H. J. (1993), *Phys. Rev. Lett.* **70**, 1195.
Moody, M. V., Canavan E. R., and Paik, H. J. (2002), submitted to *Rev. Sci. Instrum.*
Peccei, R. D. and Quinn, H. (1977), *Phys. Rev. Lett.* **38**, 1440.
Rigby, K. W., Marek, D., and Chui, T. C. P. (1990), *Rev. Sci. Inst.* **2**, 834.
Turner, M. S. (1990), *Phys. Rep.* **197**, 67.
Weinberg, S. (1978), *Phys. Rev. Lett.* **40**, 223.
Wilczek, F. (1978), *Phys. Rev. Lett.* **40**, 279.